Molecular Immunology 114 (2019) 545–552

Contents lists available at ScienceDirect

Molecular Immunology

journal homepage: www.elsevier.com/locate/molimm

Three-dimensional structure of a high affinity anti-(4-hydroxy-3-nitrophenyl)acetyl antibody possessing a glycine residue at position 95 of the heavy chain

Akihiro Nishiguchi[a,1], Nobutaka Numoto[b,1], Nobutoshi Ito[b], Takachika Azuma[c], Masayuki Oda[a,*]

[a] Graduate School of Life and Environmental Sciences, Kyoto Prefectural University, 1-5 Hangi-cho, Shimogamo, Sakyo-ku, Kyoto, 606-8522, Japan
[b] Medical Research Institute, Tokyo Medical and Dental University (TMDU), 1-5-45 Yushima Bunkyo-ku, Tokyo 113-8510, Japan
[c] Antibody Engineering Research Center, 2361-1Yamazaki, Noda, Chiba 278-0022, Japan

ARTICLE INFO

Keywords:
Antigen binding
Affinity maturation
Conformational change
Crystal structure

ABSTRACT

Antibodies possessing high affinity and specificity are desired as therapeutic reagents and biosensor materials. Such antibodies are often obtained from immunized animals through the process referred to as affinity maturation where antibody affinity increases with time after immunization. Somatic hypermutation (SHM) was shown to be involved in this process; however, structural basis of affinity maturation has not well been understood yet. We analyzed the crystal structure of a high affinity anti-(4-hydroxy-3-nitrophenyl)acetyl antibody, C6, possessing Gly at position 95 of heavy chain and 17 amino acid replacements by SHM. Here, we discuss how the amino acid residues at position 95, introduced at a junction of V_H and D_H gene segments during gene-recombination, as well as those replaced by SHM contribute to increasing the affinity by comparing the C6 structure with that of a germline low affinity antibody, N1G9, possessing Tyr at position 95.

1. Introduction

Affinity maturation is well known to increase the binding affinity of antibody towards its immunogen (Eisen and Siskind, 1964; Tonegawa, 1983; Milstein and Rada, 1995; Azuma, 1998). Structural basis of antibodies on the pathway of affinity maturation at the molecular level is critical to understand the immunological phenomena, and also provides the basis of rational protein design, for example, by suggesting ways to increase the affinity and specificity of antibodies *in vitro* (Wedemayer et al., 1997; Yin et al., 2001; Adhikary et al., 2015). The crystal structural analyses of the maturation of antibodies against a protein antigen, hen egg lysozyme (HEL), have shown that the binding affinity would be increased by subtle conformational changes in the combining site (Li et al., 2003; Cauerhff et al., 2004). Various haptens, such as (4-hydroxy-3-nitrophenyl)acetyl (NP), phosphorylcholine and 2-phenyl oxazolone, have been used to analyze the structural basis for affinity maturation (Bothwell et al., 1981; Gearhart et al., 1981; Kaartinnen et al., 1983; French et al., 1989; Alzari et al., 1990). The equilibrium association constant (K_a) of germline-type antibody towards hapten is as low as 10^5–10^6 M^{-1}, and that of affinity-matured antibody reaches 10^9 M^{-1} at maximum (Foote and Eisen, 1995; Furukawa et al., 1999; Oda and Azuma, 2000).

Several groups including ours have analyzed structural properties of anti-NP antibodies during affinity maturation (Cumano and Rajewsky, 1985; Allen et al., 1988; Azuma, 1998; Furukawa et al., 1999; Sagawa et al., 2003; Murakami et al., 2010; Oda and Azuma, 2016). Rajewsky's group reported that the Trp to Leu change at position 33 of the heavy chain, $Trp33^{H}Leu$, by somatic hypermutation is critical for the maturation from the $Tyr95^{H}$-type antibody, N1G9, which brings an increase in affinity by approximately 10-fold (Allen et al., 1988). Our group found that the amino acid (aa) residue at position 95 of the heavy chain, which corresponds to the junction of V_H and D_H segments, is critical to increase the antigen-binding affinity at the late stage of immunization (Furukawa et al., 1999). The germline anti-NP antibodies are classified into two groups, namely, $Tyr95^{H}$- and $Gly95^{H}$-type and the latter type of antibodies gain higher affinity by accumulation of somatic hypermutation (SHM) (Murakami et al., 2010). Fig. 1 shows the aa sequences of V_H and V_L regions of C6, which are compared with those of N1G9 (Bothwell et al., 1981; Cumano and Rajewsky, 1985). Hybridomas secreting C6 were prepared from C57BL/6 mice on day

* Corresponding author at: Graduate School of Life and Environmental Sciences, Kyoto Prefectural University, 1-5 Hangi-cho, Shimogamo, Sakyo-ku, Kyoto, 606-8522, Japan.
E-mail address: oda@kpu.ac.jp (M. Oda).
[1] Those authors contributed equally to the work.

https://doi.org/10.1016/j.molimm.2019.09.001
Received 4 June 2019; Received in revised form 23 July 2019; Accepted 2 September 2019

Heavy chain

```
                  10          20          30          40          50     A    60
N1G9   QVQLQQPGAE LVKPGASVKL SCKASGYTFT SYWMHWVKQR PGRGLEWIGR IDPNSGGTKYN
C6     ---------- ---------- ---T-----P Y------N-- ---------- ----G---R-S
                  70          80     ABC  90          100 ABC         110
N1G9   EKFKSKATLT VDKPSSTAYM QLSSLTSEDSAVY YCARYDYYGS SYFDYWGQGTTLT VSS
C6     ---------- -----N---- ---------- ----GKL=-Q =H--------A-- ---
```

Light chain

```
                  10          20          ABC 30          40          50          60
N1G9   QAVVTQESA= LTTSPGETVT LTCRSSTGAVTTS NYANWVQEKP DHLFTGLIGG TNNRAPGVPA
C6     ---------- ---------- ---------- --V------- -------VYS --S-V-----
                  70          80          90          100       A
N1G9   RFSGSLIGDK AALTITGAQT EDEAIYFCAL WYSNHWVFGG GTKLTVLGQ
C6     ---------- ---------A --------T- ---------- ---------
```

Fig. 1. Comparison of aa sequences of N1G9 and C6. Single dashes represent an aa residue identical with the corresponding one in N1G9. Double dashes represent deletion of aa residues. Italics represent aa residues in CDR loops defined by Kabat (Kabat et al., 1991). The aa residues at 33 and 95 of heavy chain are indicated in bald. The aa numbering is based on the Kabat system (Kabat et al., 1991).

104 after immunization of NP-chicken γ-globulin (NP-CGG) with alum followed by multiple injections with NP-CGG in PBS (Azuma et al., 1984). C6 has K_a of 3.3×10^7 M^{-1} for ε-(NP-amino)caproic acid (NP-Cap) (Furukawa et al., 1999). A hybridoma producing N1G9 was kindly donated by Rajewsky, which was prepared on day 7 after immunization of NP-CGG. N1G9 is encoded by canonical gene segments such as *V186.2*, *DFL16.1* and J_H2 for heavy chain genes and $V_\lambda1$ and $J_\lambda1$ for light chain genes without SHM, it was employed as a prototype of anti-NP antibodies from C57BL/6 mouse (Bothwell et al., 1981; Cumano and Rajewsky, 1985). Crystal structures of N1G9 in the presence and absence of NP determined at 2.4 Å resolution (PDB codes; 1NGP and 1NGQ, respectively) has been reported previously (Mizutani et al., 1995). The NP binding affinities of N1G9 and C6, K_a values towards monovalent antigen of NP conjugated HEL under physiological conditions, were determined to be 1.37×10^5 M^{-1} and 1.30×10^7 M^{-1}, respectively (Oda and Azuma, 2016). Since anti-NP antibodies possessing $Gly95^H$ are able to attain higher affinities through affinity maturation while those possessing $Tyr95^H$ are not (Murakami et al., 2010), comparison of crystal structure between $Tyr95^H$-type N1G9 (Mizutani et al., 1995) and $Gly95^H$-type C6 is of interest from the point of view that how anti-NP antibodies possessing $Gly95^H$ gain high affinity at atomic level.

In this study, we determined the crystal structure of a single-chain Fv (scFv) antibody of C6, which is the first report for the structure of $Gly95^H$-type anti-NP antibodies. Since scFv antibodies of N1G9, C6, and their $Trp33^H$Leu mutants showed little difference in terms of the physical and functional properties (Murakami et al., 2010; Sato et al., 2016, 2017) compared with parent antibodies, we consider that C6 scFv represents the antigen-combining site of intact antibodies. Together with the abundant results of anti-NP antibodies during the affinity maturation, the present results shed light on the role of $Gly95^H$ on the antibody structure based on physical and functional properties.

2. Materials and methods

2.1. Purification of C6 scFv and its crystallization in complex with NP

C6 scFv over-expressed in the insoluble fraction *by E. coli* was solubilized using 8 M urea and refolded by stepwise dilution of urea from 8 M to 0 M, *via.* 4, 2, 1 M, as reported procedure (Sato et al., 2016). The refolded protein was purified using a column of NP conjugated to bovine serum albumin. The concentration of C6 scFv was spectrophotometrically determined using molar absorption coefficient of 5.64×10^4 M^{-1} cm^{-1} at 280 nm. Crystallization conditions were screened by the sparse matrix method using commercially available screening kits (Hampton Research) with the hanging-drop vapor-diffusion method at 4 °C (Jancarik and Kim, 1991).

2.2. X-ray diffraction experiments and analysis

X-ray diffraction experiments were performed at the beamline BL-1A at KEK-PF. The data were processed and scaled using the program XDS (Kabsh, 2010) and truncated by the CCP4 program suite (Winn et al., 2011). For further refinement, 5% of the reflections were set apart as a random test set to calculate the R_{free} values.

The structure of another scFv of the engineered neutralizing antibody m18 (Leysath et al., 2009, PDB code; 3ET9) was used as a search model to determine the initial phases by the molecular replacement method using the program PHASER (McCoy et al., 2007). Several cycles of manual model rebuilding and refinement were performed by using the program COOT and the program PHENIX, respectively (Emsley et al., 2010; Adams et al., 2010). The refined model was validated by the program MOLPROBITY (Chen et al., 2010). The statistics for data collection and refinement are summarized in Table 1. The figures were prepared with the program PYMOL (http://www.pymol.org/) and LigPlot$^+$ (Laskowski and Swindells, 2011).

3. Results

3.1. Comparison of the aa sequences between C6 and N1G9

A comparison of the aa sequences between C6 and N1G9 reveals that they possesses similar first and second complementarity-determining regions of heavy chains (H-CDR1 and H-CDR2), although variations induced by SHM are observed, and different H-CDR3 in both length and aa sequences. This is attributed to the usage of the same V_H gene segment (*V186.2*) and different D_H gene segments, *DFL16.1* for N1G9 vs *DQ52* for C6, and to the action of terminal deoxyribonucleotidyl transferase (TdT) during gene recombination (Benedict et al., 2000). In particular, a profound diversity of the aa residue at 95^H that corresponded to the boundary of the V_H-D_H junction was observed (Kabat et al., 1991; Hofle et al., 2000), namely, C6 has the $Gly95^H$, while N1G9 the $Tyr95^H$. In addition, deletions at positions 98 and 100A made C6 H-CDR3 shorter than that of N1G9 (Fig. 1). Since antibodies possessing $Gly95^H$ paired with $His102^H$ like C6 were found in hybridomas prepared from activation-induced cytidine deaminase$^{-/-}$ mice (Murakami et al., 2013), we considered $Gly95^H$ and $His102^H$ were introduced by the action of TdT but not by SHM. First, we wanted to know how the difference of H-CDR3 primary structure affected the

Table 1
Data collection and refinement statistics. Values in parentheses are for the highest resolution shell.

Data collection	
Wavelength (Å)	1.0000
Space group	*P*1
Unit-cell parameters	
a / *b* / *c* (Å)	37.4 / 46.8 / 74.6
α / *β* / γ (º)	88.2 / 103.8 / 112.0
Resolution (Å)	50-1.65 (1.75-1.65)
No. of observations	190,998
No. of unique reflections	52,628
Completeness (%)	96.2 (94.1)
Average $I/\sigma(I)$	11.2 (2.1)
Redundancy	3.6 (3.5)
R_{sym} (%)	7.3 (58.6)
$CC_{1/2}$ (%)	99.8 (71.6)
Refinement	
R (%)	16.7
R_{free} (%)	19.6
Number of molecule in asymmetric unit	2
Average *B* factor (Å^2)	22.6
r.m.s. deviation from ideal	
Bonds (Å)	0.007
Angles (º)	0.87
Ramachandran plot	
Favored region (%)	96.4
Allowed region (%)	3.6
Outlier region (%)	0

conformation of antigen-combining sites and hapten-antibody interaction. The variation in aa sequences between N1G9 and C6 by SHM was observed at 17 positions, 9 in V_H region and 8 in V_L region, respectively (Fig. 1). Among these mutations, 4 mutations, Ser31^{H}Tyr, Ser54^{H}Gly, Lys58^{H}Arg and Asn60^{H}Ser occurred in H-CDRs. Similarly, 5 mutations, Ala33^{L}Val, Gly50^{L}Ser, Asn53^{L}Ser, Ala55^{L}Val and Ala89^{L}Thr occurred in L-CDRs, and Ala24^{H}Thr, Thr30^{H}Pro, Lys38^{H}Asn, Ser76^{H}Asn, Thr108^{H}Ala, Ile48^{L}Val, Gly49^{L}Tyr and Thr80^{L}Ala occurred in framework regions, respectively. Since affinity maturation is shown to proceed by accumulation of SHM, it is of interest to know how these 17 mutations are involved in the interaction with NP.

3.2. Crystallization and structure determination

For crystallization, C6 scFv was concentrated to 0.2 mM in 40 mM phosphate buffer (pH 7.3) and mixed with NP at molar ratio of 1:1. Crystals were obtained in 0.14 M lithium sulfate monohydrate, 0.07 M Tris hydrochloride at pH 8.5 and 21% w/v polyethylene glycol 4000. The crystals appeared within 2 weeks and grew to the maximum dimensions of 0.02 mm × 0.02 mm × 0.2 mm.

The crystal structure of C6 scFv complexed with NP was determined at 1.65 Å resolution (Fig. 2, Table 1). An asymmetric unit contains two molecules of C6 scFv. The overall structures of Fv region is as that of the canonical antibodies. Comparison between the two molecules in the asymmetric unit showed that the loop geometry of L-CDR3 is slightly different (Fig. 2), while the structures of other regions are almost the same. Root mean square deviation (RMSD) of main-chain is 0.53 Å. Because one molecule matches well with the structure of NP-bound N1G9 even at the L-CDR3, we will use this protomer for further analysis.

3.3. Antigen recognition mechanism of C6

Crystallographic analyses showed that the antigen combining site of C6 is created by aa residues residing in CDRs such as Trp33^H and His35^H in H-CDR1; Arg50^H and Arg58^H in H-CDR2; Gly99^H, Leu97^H and His102^H in H-CDR3; Tyr32^L in L-CDR1; Trp91^L and Trp96^L in L-CDR3, respectively (Fig. 3). Comparison of the structural data of C6 with those of germline antibody N1G9 (Mizutani et al., 1995) revealed only marginal differences between these two antibodies in terms of the positions of the aa residues in H-CDR1, H-CDR2 and L-CDR3 such as Trp33^H, His35^H, Arg50^H, Arg58^H (Lys58^H), Trp91^L and Trp96^L, which reside close to NP molecules in the antigen combing sites. The phenyl group of NP is recognized and trapped by π-π stacking with Trp91^L in both C6 and N1G9. It appeared that the contact geometry of the π-π stacking in C6 is more preferable to that of N1G9, owing to the almost complete parallel geometry of the two aromatic rings and appropriate slipped stacking geometry in C6 (Fig. 3C). Trp33^H could contribute to CH-π interaction with NP in both C6 and N1G9. Excluding H-CDR3, the RMSD of main-chain atoms between Fv regions of N1G9 and C6 is 0.81 Å, indicating that there are no remarkable conformational differences in the NP-antibody complexes apart from the H-CDR3 structure.

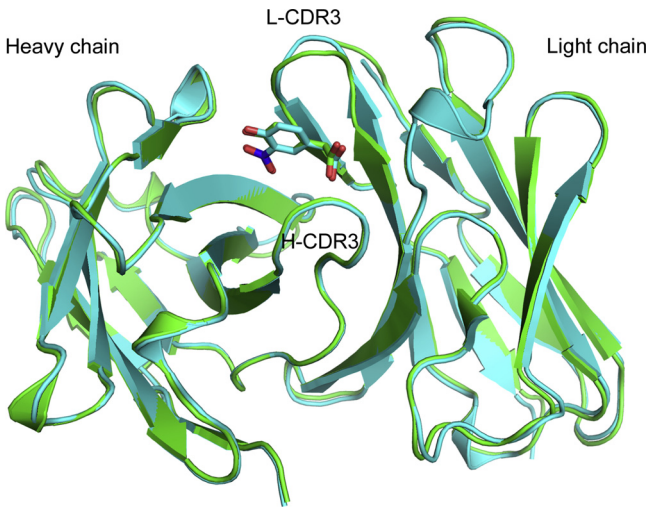

Fig. 2. Crystal structure of C6 scFv in complex with NP (shown as stick model). Two protomers in the asymmetric unit are drawn as green and cyan. The conformation of L-CDR3 of green protomer well match that of N1GP. (For interpretation of the references to colour in these figure legends, the reader is referred to the web version of this article.)

Contrast to the similarity in the structure of H-CDR1 and H-CDR2, a large difference was observed in that of H-CDR3. Namely, Leu97^H, Gly99^H and His102^H interact with NP in C6; while Tyr95^H, Tyr97^H and Ser101^H contact with NP in N1G9 (Fig. 3A). Bulky side-chains of Tyr95^H and Tyr97^H occupy in N1G9 but Gly95^H occurs in C6, which makes a large empty space enabling His102^H large movement and compensation for this space (Fig. 3A). This steric compensation by His102^H seems to induce the rearrangement of the recognition residues; the side-chain of His102^H and the main-chain nitrogen of Gly99^H form hydrogen bonds to the carboxyl group of NP in C6, whereas the side-chain of Tyr95^H and Ser101^H are responsible for forming hydrogen bonds and recognition of the carboxyl group of NP in N1G9. It seems to be more ideal geometry for hydrogen bond in C6 than those of N1G9 because of longer distance between the side-chain O atom of Ser101^H and carboxyl group of NP. As described, the aa residues introduced by SHM did not appear to involve in the interaction with NP except for Arg58^H, although they occurred at 17 positions.

3.4. Effects of Lys58^{H}Arg on the interaction with hapten

Lys58^{H}Arg is the only mutation involved directly in the interaction with NP, which accompanies the substitution of ε-ammonium group of Lys to the guanidinium group of Arg, both of which are positively charged at physiological pH. The hydroxyl group of NP is recognized by the hydrogen bond with Arg50^H and Arg58^H in C6 to a similar extent as with Arg50^H and Lys58^H in N1G9. The aa residues involved in the

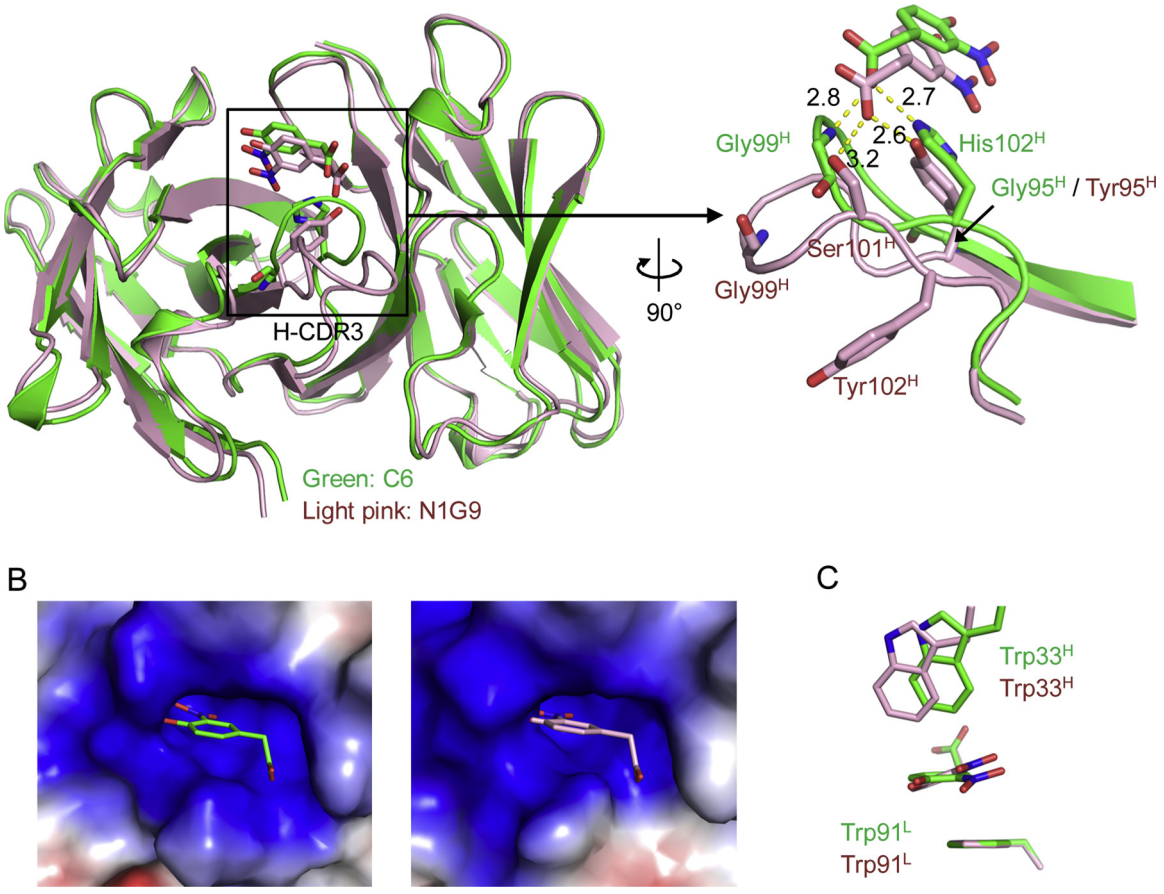

Fig. 3. (A) Superposition of the overall structure of C6 scFv (green) and the Fv region of N1G9 (light pink, PDB ID 1NGP). The color scheme is the same in subsequent figures. H-CDR3 loops and bound NP are indicated as black box. The key aa residues of $His102^{H}$ of C6 and $Tyr95^{H}$ of N1G9 are also shown as stick model. Right panel is close up view of the comparison of H-CDR3. Hydrogen bonds at the carboxyl group of NP are shown as yellow dashed lines. (B) Electrostatic potentials around NP binding pockets of C6 (left) and N1G9 (right). Electrostatic potentials were calculated using the program APBS (Baker et al., 2001) and are represented by PYMOL (http://www.pymol.org/), with the color of the surface potentials in the scale ranging from red (–3.0 kT/e) to blue (3.0 kT/e). (C) Comparison of the contacting geometry of the π-π stacking between $Trp91^{L}$ and NP. $Trp33^{H}$ could be contact with CH-π interaction. Each $Trp91^{L}$ of C6 and N1G9 are superposed.

recognition of the nitro group of NP in C6 are $Trp96^{L}$, $Arg50^{H}$ and $Arg58^{H}$; the hydrogen bond between the nitro group and $Trp96^{L}$ was at an ideal distance, whereas it is slightly longer for those of $Arg50^{H}$ and $Arg58^{H}$. In the case of N1G9; $His35^{H}$, $Arg50^{H}$ and $Trp96^{L}$ form hydrogen bonds with nitro group of NP. $His35^{H}$ contacts the nitro group in N1G9 with an ideal distance for hydrogen bond, but the side-chain of $His35^{H}$ in C6 was flipped and away from the nitro group (3.2 Å), so that $His35^{H}$ of C6 could not directly interact with NP. It should be noted that $His35^{H}$ of C6 formed hydrogen bond with $His102^{H}$ that interacts with the carboxyl group of NP. The role of $His35^{H}$, therefore, seemed to be different; hydrogen bonding with nitro group of NP in N1G9 and stabilizing $His102^{H}$ conformation in C6. $His35^{H}$ and $Arg50^{H}$ in N1G9 tightly form hydrogen bond with the nitro group of NP, whereas the corresponding interactions in C6 appear to be slightly weakened than those of N1G9. To summarize, interactions of C6 with carboxyl groups and aromatic rings of NP molecules are enhanced, while those with the hydroxyl or nitro groups appear to be similar or slightly weakened compared with N1G9 (Fig. 4).

More sophisticated recognition mechanism for the carboxyl group of NP in C6 is suggested from the analysis of the charge distribution of molecular surface (Fig. 3B). Highly positive charge patch around the carboxyl and nitro groups of bound NP in C6 can tightly recognize both the negatively charged carboxyl and the oxygen atoms of nitro group. $Arg58^{H}$, $Lys96^{H}$ and $His102^{H}$ appear to contribute to the formation of the positive charged patch around carboxyl group. This electrostatic environment appears to be slightly weaker in N1G9 than that in C6. Therefore, the recognition manner of the carboxyl group in C6 seems to be more ideal in terms of geometry for the hydrogen bond and molecular surface charge distribution than N1G9.

3.5. Contribution of other mutations to raise affinity

It is rather surprising that 16 out of 17 replacements of aa residues by SHM are not involved in the direct interactions by forming hydrogen-bonds or through electrostatic force (Fig. 5). Despite occurrence of $Ser54^{H}Gly$ and $Asn60^{H}Ser$ in the same H-CDR2 as $Lys58^{H}Arg$, there are no hydrogen bonds or hydrophobic interactions between these aa residues and NP. However, although most of mutations occur apart from the antigen combining sites and spread over the C6 structure (Fig. 5), $Gly49^{L}Tyr$ seems to affect H-CDR3 conformation, especially at $His102^{H}$. Such a replacement accompanied with a volume change of side-chains is also observed in $Gly50^{L}Ser$ and $Ala55^{L}Val$, suggesting that these mutations in light chains contribute to alter the combining site conformation. These results are in accord with a previous observation that SHM in light chains is essential to express the full NP binding activity of C6 (Murakami et al., 2010).

4. Discussion

First, we asked how H- and L-CDRs created the gross structure of antigen combining sites and found that H-CDR1, H-CDR2, H-CDR3, L-CDR1 and L-CDR3 are involved in the construction of combining sites, while L-CDR2 is not. Comparison of the CDR structures revealed that only marginal differences are observed in H-CDR1, H-CDR2 and L-

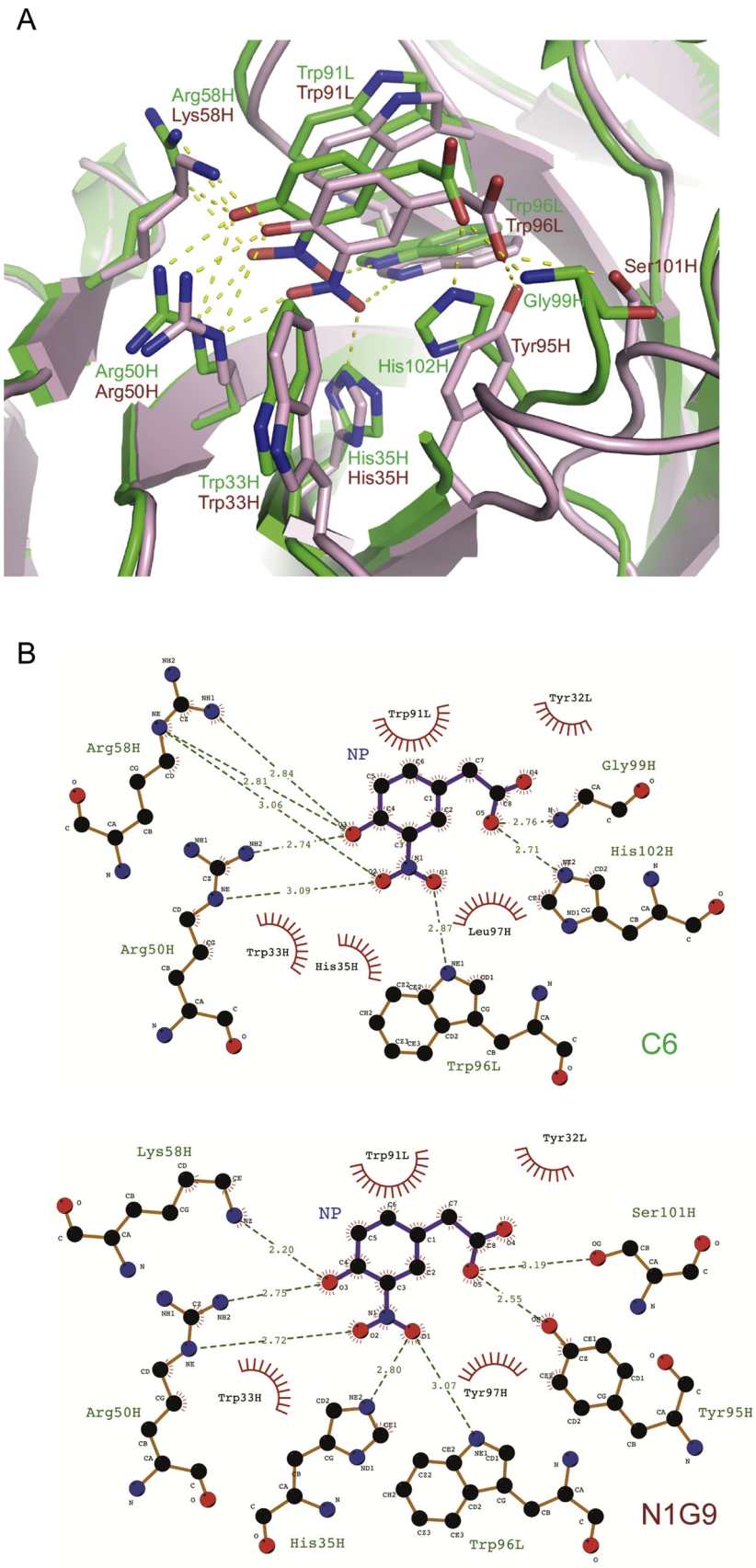

Fig. 4. (A) Close up view of the NP binding sites of C6 and N1G9. Polar contacts are indicated as yellow dashed lines. (B) Antigen-protein interaction diagrams of C6 and N1G9.

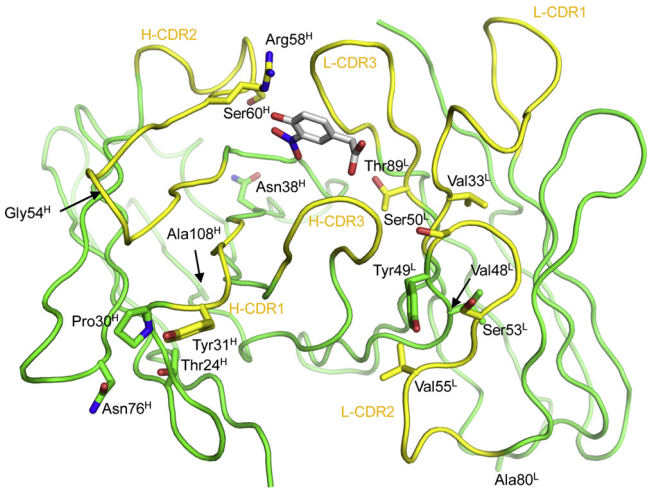

Fig. 5. Residues replaced by SHM. The stick models are side-chains of 17 SHM residues in C6 and bound NP. CDR regions are indicated as yellow.

CDR3 between C6 and N1G9. Although total 4 mutations occur in H-CDR1 and H-CDR2, they are likely to provide little influence on the conformation. Next, we examined whether the differences in the H-CDR3 sequences affect the structure of antigen combining sites and the interaction with NP molecules. The aa residues, Leu97^{H}, Gly99^{H}, His102^{H} in C6 H-CDR3 and Tyr95^{H}, Tyr97^{H}, Ser101^{H} in N1G9 H-CDR3 involve in the construction of the antigen combining site. In these residues, Tyr95^{H} and Ser101^{H} in N1G9 reside at V_H-D_H and D_H-J_H junctions and are involved as key elements in the construction of antigen combining sites and formation of NP-antibody complex. However, in the case of C6, Gly95^{H} at V_H-D_H junction are not involved, but Gly99^{H} and His102^{H} at D_H-J_H junction participate in the interaction with NP. In addition to the aa residues in H-CDR3, Trp96^{L} at V_L-J_L junction in L-CDR3 are involved in the combining sites of both C6 and N1G9 (Fig. 4), which is in agreement with a previous report that the aa residue at position 96^{L} provided large effects on the NP-antibody interaction (Azuma et al., 1984). These results indicate that the aa residues in H-CDR3 and L-CDR3, especially occurring at the junction of gene segments, play an important role in the interaction with antigens. In fact, it was reported that an anti-dinitrophenyl (DNP) antibody, SPE7, which is encoded by exactly same gene segments as N1G9 but possesses different aa residues, Met95^{H} at V_H-D_H junction, Tyr102^{H} at D_H-J_H junction and Leu96^{L} at V_L-J_L junction, respectively, shows no binding to NP but high affinity to DNP (James and Tawfik, 2003). However, a question arises; why do both C6 and N1G9 show the same specificity despite the difference in H-CDR3 aa sequences including V_H-D_H and D_H-J_H junctions? The answer can be provided by the results in Fig. 4, which shows that hydrogen bonds between the oxygen atom of NP carboxyl group and Gly99^{H} and His102^{H} in C6 are replaced by Tyr95^{H} and Ser101^{H} in N1G9 without changing the formation of hydrogen bonds with NP. This is also a reason why antibodies possessing either Tyr95^{H} or Gly95^{H} are predominantly observed in hybridomas secreting anti-NP antibodies (Furukawa et al., 1999). In addition to the specificity, a germline Gly95^{H}-type and Tyr95^{H}-type anti-NP antibodies are similar in magnitude of affinities. A Gly95^{H}-type antibody, 9 TG, was reported to possess K_a of ~10^6 M^{-1} for NP-ε-amino caproic acid (Furukawa et al., 2007), which was similar to that of N1G9, $K_a = 5.5 \times 10^5$ M^{-1} (Torigoe et al., 1995). These results suggest that the difference, if any, in the H-CDR3 sequences provide only small effect on the affinity and specificity of germline anti-NP antibodies.

In spite of such similarity in specificity and affinity as described above, Furukawa et al. (1999) showed the final affinities (ceiling affinities) through the process of affinity maturation are different between Tyr95^{H}-type and Gly95^{H}-type antibodies; the Tyr95^{H}-type antibodies attain the K_a values of ~10^7 M^{-1} at most, while the Gly95^{H}-type antibodies gain higher affinities than the former and some Gly95^{H}-type antibodies show K_a values of ~10^9 M^{-1}. Although the mechanism of Gly95^{H}-type antibodies to gain higher affinity than Tyr95^{H}-type was not understood yet, Kim et al. (1991) reported that large varieties of loop conformations are observed when the first aa residue was Gly based on a simulation calculation. The present results suggest that a large conformational freedom in H-CDR3 of Gly95^{H}-type antibodies, due to a small side-chain of Gly95^{H} and short H-CDR3 length, allows the fine tuning of combining site structure to have better contact with NP molecule by accumulating SHM (Sagawa et al., 2003; Furukawa et al., 2007). In the case of Tyr95-type, a bulky side-chain of Tyr95^{H} and its direct interaction with NP would not allow the alteration of combining site configuration.

The SHM occurs at 17 locations in C6 (Fig. 1). Among these, Lys58^{H}Arg in H-CDR2 is the only mutation involved directly in the interaction with NP through formation of hydrogen bonds. Since this mutation is observed widely in Gly95^{H}-type antibodies, it is referred to as a parallel mutation, and was expected to be a common strategy to raise the affinity of this type antibodies. As Lys58^{H}Arg was not found in Tyr95^{H}-type antibodies, it is considered to provide a negative effect on the NP-antibody interaction. The Trp33^{H}Leu in H-CDR1 represents another example of a parallel mutation, which causes an increase ~10-fold affinity in the interaction with NP and is considered to be a strategy of affinity maturation of Tyr95^{H}-type antibodies (Allen et al., 1988), since the same mutation provides reverse effect on the affinity of Gly95^{H}-type antibodies (Murakami et al., 2010: Sato et al., 2017). The reciprocal effect of Lys58^{H}Arg or Trp33^{H}Leu on the respective types of antibodies suggests that H-CDR3 structure, especially the aa residues at position 95, link these parallel mutations, i.e., the strategy of affinity maturation. It is likely that the combining sites are sustained by a delicate balance and mutual dependence of aa residues, whose replacements by SHM in total possibly bring about drastic effect on the antigen-antibody interaction in both heavy and light chains, as described below. Therefore, the selected aa residues such as Lys58^{H} for Gly95^{H}-type and Trp33^{H} for Tyr95^{H}-type antibodies can change by SHM. In fact, a mutation, Arg50^{H}Gly in H-CDR2 of an anti-NP antibody, obtained from a culture cell line B1-8.δ1, was reported to result in the change of the specificity from NP to DNP (Bruggemann et al., 1986).

Although the aa residues introduced by SHM, except for Arg58^{H}, are not involved in the construction of antigen combining sites (Fig. 5), the fine configuration of unmutated aa residues was different between N1G9 and C6; His35^{H} forms a hydrogen bond with NP in N1G9, while the direction of His35^{H} side-chain is altered and unable to form the hydrogen bond with NP, which, in turn, enables better contact of His102^{H} with NP in C6. Such a difference in fine configuration is supposed to be created by aa residues introduced by SHM at locations distant from combining sites. For example, the Gly49^{L}Tyr in framework region seems to contribute to altering the H-CDR3 conformation, especially around His102^{H}. Previously, the contribution of aa replacements to the increase in a Gly95^{H}-type antibody affinity was estimated by preparing recombinant antibodies (Furukawa et al., 2007), which shows that 6 mutations in the heavy chain including Lys58^{H}Arg are responsible for increase in affinity of ~40% and mutations in the light chain are that of ~60%, respectively. Murakami et al. (2010) also showed the importance of the mutations in C6 light chain to express full binding activity to antigens. Present study supports the results Taketani et al. (1995), who, based on aa sequence analyses, predicted that the aa residues introduced by SHM may act by refining orientation of the conserved aa residues in CDRs and resulted in an increase in affinity. There is a lot of example that the mutation of the residue away from the functional site greatly influences the function by affecting the stability or structural dynamics of the protein (Naganathan, 2019). In order to verify these effects by such as a computational method, higher resolution structures are required for both N1G9 and C6. The NP binding affinity of C6 is ~10^7 M^{-1} and is not very high among Gly95^{H}-type antibodies (Furukawa et al., 1999). The structural analysis for antibodies

with higher NP binding affinity is under progress, which will provide more detailed information how Gly95^{H} and additional mutations can contribute to the increased affinity.

Previously, our study on structural dynamics of C6 scFv using diffracted X-ray tracking (DXT) experiments showed that the fluctuation in C6 scFv is suppressed upon antigen binding (Sato et al., 2016). The DXT system could monitor the real-time motion by observations of X-ray diffracted spots from a gold-nanocrystal, tightly bound to the biomolecule such as C6 scFv (Sato-Tomita et al., 2018). In addition, thermal stability of C6 scFv is much lower than that of N1G9 scFv, which increases up to the same level of N1G9 scFv upon antigen binding (Sato et al., 2017). In the case of N1G9, H-CDR3 seems to be stabilized by π-π stacking between Tyr97^{H} and Trp33^{H} (H-CDR1) and by edge-to-face π-π interaction between Tyr97^{H} and Tyr98^{H}. No significant structural changes are observed in H-CDR3 between NP-bound and free forms. In the case of C6-NP complex, NP molecule is well accommodated in the combining site and provided stabilization effect to H-CDR3, which results in increasing thermal stability of the complex. To resolve the low thermal stability of free C6, which shows higher affinity to NP, additional studies including crystallographic analysis of antigen-free C6 together with its structural dynamics would be needed.

5. Conclusions

Although a line of evidence showed that antibody affinity maturation proceeds by induction of SHM, it is not yet verified how the aa residues introduced by SHM contribute to raising affinity without changing specificity at atomic level. The three-dimensional structure of C6 possessing 17 mutations, 9 in CDRs and 8 in framework regions, respectively, revealed that only one mutation in H-CDR2, Lys58^{H}Arg, involves directly in the formation of hydrogen bond with NP. Other mutations occur distant from the combining sites and contribute to raising affinity by refining the orientation of unmutated aa side-chains in antigen combining sites.

The atomic coordinate and structure factor (code 6K4Z) have been deposited in the Protein Data Bank (pdbj.org).

Declaration of Competing Interest

The authors declare that they have no conflicts of interest with the contents of this article.

Acknowledgements

The authors thank Takanori Yamaoka of Kyoto Prefectural University for technical support. This study was supported by JSPS KAKENHI Grant Number 18K06161 and Nanken-Kyoten, Tokyo Medical and Dental University. The X-ray crystal structure analysis has been performed under the approval of the Photon Factory Program Advisory Committee (Proposal No. 2016G638 and 2017G514).

References

Adams, P.D., Afonine, P.V., Bunkóczi, G., Chen, V.B., Davis, I.W., Echols, N., Headd, J.J., Hung, L.W., Kapral, G.J., Grosse-Kunstleve, R.W., McCoy, A.J., Moriarty, N.W., Oeffner, R., Read, R.J., Richardson, D.C., Richardson, J.S., Terwilliger, T.C., Zwart, P.H., 2010. PHENIX: a comprehensive Python-based system for macromolecular structure solution. Acta Cryst. D66, 213–221.

Adhikary, R., Yu, W., Oda, M., Walker, R.C., Chen, T., Stanfield, R.L., Wilson, I.A., Zimmermann, J., Romesberg, F.E., 2015. Adaptive mutations alter antibody structure and dynamics during affinity maturation. Biochemistry 54, 2085–2093.

Allen, D., Simon, T., Sablitzky, F., Rajewsky, K., Cumano, A., 1988. Antibody engineering for the analysis of affinity maturation of an anti-hapten response. EMBO J. 7, 1995–2001.

Alzari, P.M., Spinelli, S., Mariuzza, R.A., Boulot, G., Poljak, R.J., Jarvis, J.M., Milstein, C., 1990. Three-dimensional structure determination of an anti-2-phenyloxazolone antibody: the role of somatic mutation and heavy/light chain pairing in the maturation of an immune response. EMBO J. 9, 3807–3814.

Azuma, T., Igras, V., Reilly, E.B., Eisen, H.N., 1984. Diversity at the variable-joining region boundary of λ light chains has a pronounced effect on immunoglobulin ligand-binding activity. Proc. Natl. Acad. Sci. U.S.A. 81, 6139–6143.

Azuma, T., 1998. Somatic hypermutation in mouse λ chains. Immunol. Rev. 162, 97–105.

Baker, N.A., Sept, D., Joseph, S., Holst, M.J., McCammon, J.A., 2001. Electrostatics of nanosystems: application to microtubules and the ribosome. Proc. Natl. Acad. Sci. U.S.A. 98, 10037–10041.

Benedict, C.L., Gilfillan, S., Thai, T.H., Kearney, J.F., 2000. Terminal deoxynucleotidyl transferase and repertoire development. Immunol. Rev. 175, 150–157.

Bothwell, A.L.M., Paskind, M., Reth, M., Imanishi-Kari, T., Rajewsky, K., Baltimore, D., 1981. Heavy chain variable region contribution to the NP^{b} family of antibodies: somatic mutation evident in a γ2a variable region. Cell 24, 625–637.

Bruggemann, M., Muller, H.-J., Burger, C., Rajewsky, K., 1986. Idiotypic selection of an antibody mutant with changed hapten binding specificity, resulting from a point mutation in position 50 of the heavy chain. EMBO J. 5, 1561–1566.

Cauerhff, A., Goldbaum, F.A., Braden, B.C., 2004. Structural mechanism for affinity maturation of an anti-lysozyme antibody. Proc. Natl. Acad. Sci. U.S.A. 101, 3539–3544.

Chen, V.B., Arendall 3rd, W.B., Headd, J.J., Keedy, D.A., Immormino, R.M., Kapral, G.J., Murray, L.W., Richardson, J.S., Richardson, D.C., 2010. MolProbity: all-atom structure validation for macromolecular crystallography. Acta Cryst D66, 12–21.

Cumano, A., Rajewsky, K., 1985. Structure of primary anti-(4-hydroxy-3-nitrophenyl) acetyl (NP) antibodies in normal and idiotypically suppressed C57BL/6 mice. Eur. J. Immunol. 15, 512–520.

Eisen, H.N., Siskind, G.W., 1964. Variation in affinities of antibody during immune response. Biochemistry 3, 996–1008.

Emsley, P., Lohkamp, B., Scott, W.G., Cowtan, K., 2010. Features and development of coot. Acta Crystallogr. D Biol. Crystallogr. 66, 486–501.

Foote, J., Eisen, H.N., 1995. Kinetic and affinity limits on antibodies produced during immune responses. Proc. Natl. Acad. Sci. U.S.A. 92, 1254–1256.

French, D.L., Laskov, R., Scharff, M.D., 1989. The role of somatic hypermutation in the generation of antibody diversity. Science 244, 1152–1157.

Furukawa, K., Akasako-Furukawa, A., Shirai, H., Nakamura, H., Azuma, T., 1999. Junctional amino acids determine the maturation pathway of an antibody. Immunity 11, 329–338.

Furukawa, K., Shimizu, T., Murakami, A., Kono, R., Nakagawa, M., Sagawa, T., Yamato, I., Azuma, T., 2007. Strategy of affinity maturation of an antibody with high evolvability to (4-hydroxy-3-nitrophenyl)acetyl hapten. Mol. Immunol. 44, 2346–2445.

Gearhart, P.J., Johnson, N.D., Douglas, R., Hood, L., 1981. IgG antibodies to phosphorylcholine exhibit more diversity than their IgM counterparts. Nature 291, 29–34.

Hofle, M., Linthicum, D.S., Ioerger, T., 2000. Analysis of diversity of nucleotide and amino acid distributions in the VD and DJ joining regions in Ig heavy chains. Mol. Immunol. 37, 827–835.

James, L.C., Tawfik, D.C., 2003. The specificity of cross-reactivity: promiscuous antibody binding involves specific hydrogen bonds rather than nonspecific hydrophobic stickiness. Protein Sci. 12, 2183–2193.

Jancarik, J., Kim, S.H., 1991. Sparse matrix sampling: a screening method for crystallization of proteins. J. Appl. Cryst. 24, 409–411.

Kaartinnen, M., Griffiths, G.M., Markham, A.F., Milstein, C., 1983. mRNA sequences define an unusually restricted IgG response to 2-phenyl oxazolone and its early diversification. Nature 304, 320–324.

Kabat, E.A., Reed-Miller, M., Perry, H.M., Gottesman, K.S., 1991. Sequences of proteins of immunological interest. Department of Health and Human Services, Public Health Service, 5th ed. National Institutes of Health, Bethesda, MD.

Kabsh, W., 2010. Xds. Acta Crystallogr. D Biol. Crystallogr. 66, 125–132.

Laskowski, R.A., Swindells, M.B., 2011. LigPlot^{+}: multiple ligand-protein interaction diagrams for drug discovery. J. Chem. Inf. Model. 51, 2778–2786.

Leysath, C.E., Monzingo, A.F., Maynard, J.A., Barnett, J., Georgiou, G., Iverson, B.L., Robertus, J.D., 2009. Crystal structure of the engineered neutralizing antibody M18 complexed to domain 4 of the anthrax protective antigen. J. Mol. Biol. 387, 680–693.

Li, Y., Li, H., Yang, F., Smith-Gill, S.J., Mariuzza, R.A., 2003. X-ray snapshots of the maturation of an antibody response to a protein antigen. Nat. Struct. Biol. 10, 482–488.

McCoy, A.J., Grosse-Kunstleve, R.W., Adams, P.D., Winn, M.D., Storoni, L.C., Read, R.J., 2007. Phaser crystallographic software. J. Appl. Cryst. 40, 658–674.

Milstein, C., Rada, C., 1995. The maturation of the antibody response. In: Honjo, T., Alt, F.W. (Eds.), Immunoglobulin Genes, 2nd ed. Academic Press, pp. 57–81.

Mizutani, R., Miura, K., Nakayama, T., Shimada, I., Arata, Y., Satow, Y., 1995. Three-dimensional structures of the Fab fragment of murine N1G9 antibody from the primary immune response and of its complex with (4-hydroxy-3-nitrophenyl)acetate. J. Mol. Biol. 254, 208–222.

Murakami, A., Takahashi, Y., Nishimura, M., Shimizu, T., Azuma, T., 2010. The amino acid residue at position 95 and the third CDR region in the H chain determine the ceiling affinity and the maturation pathway of an anti-(4-hydroxy-3-nitrophenyl) acetyl antibody. Mol. Immunol. 48, 48–58.

Murakami, A., Moriyama, H., Osako-Kabasawa, Endo, K., Nishimura, M., Udaka, K., Muramatsu, M., Honjo, T., Shimizu, T., 2013. Low-affinity IgM antibodies lacking somatic hypermutations are produced in the secondary response of C57BL/6 mice to (4-hydroxy-3-nitrophenyl)acetyl hapten. Int. Immunol. 26, 195–208.

Naganathan, A.N., 2019. Modulation of allosteric coupling by mutations: from protein dynamics and packing to altered native ensembles and function. Curr. Opin. Struct. Biol. 54, 1–9.

Oda, M., Azuma, T., 2000. Reevaluation of stoichiometry and affinity/avidity in interactions between anti-hapten antibodies and mono- or multi-valent antigens. Mol. Immunol. 37, 1111–1122.

Oda, M., Azuma, T., 2016. Affinity maturation of anti-(4-hydroxy-3-nitrophenyl)acetyl antibodies accompanies a modulation of antigen specificity. Mol. Immunol. 70, 8–12.

Sagawa, T., Oda, M., Ishimura, M., Furukawa, K., Azuma, T., 2003. Thermodynamic and kinetic aspects of antibody evolution during the immune response to hapten. Mol. Immunol. 39, 801–808.
Sato, Y., Tanaka, Y., Inaba, S., Sekiguchi, H., Maruno, T., Sasaki, Y.C., Fukada, H., Kobayashi, Y., Azuma, T., Oda, M., 2016. Structural dynamics of a single-chain Fv antibody against (4-hydroxy-3-nitrophenyl)acetyl. Int. J. Biol. Macromol. 91, 151–157.
Sato, Y., Inaba, S., Fukada, H., Azuma, T., Oda, M., 2017. Pronounced effect of hapten binding on thermal stability of an anti-(4-hydroxy-3-nitrophenyl)acetyl antibody possessing a glycine residue at position 95 of the heavy chain. Mol. Immunol. 85, 130–136.
Sato-Tomita, A., Sekiguchi, H., Sasaki, Y.C., 2018. Progression of 3D protein structure and dynamics measurements. J. Phys. Society Japan 87, 061015.
Taketani, M., Naitoh, A., Motoyama, N., Azuma, T., 1995. Role of conserved amino acid residues in the complementarity determining regions on hapten-antibody interaction of anti-(4-hyrdroxy-3-nitrophenyl)acetyl antibodies. Mol. Immunol. 32, 983–990.
Tonegawa, S., 1983. Somatic generation of antibody diversity. Nature 302, 575–581.
Torigoe, H., Nakayama, T., Imazato, M., Shimada, I., Arata, Y., Sarai, A., 1995. The affinity maturation of anti-4-hydroxy-3-nitrophenylacetyl mouse monoclonal antibody. A calorimetric study of the antigen-antibody interaction. J. Biol. Chem. 270, 22218–22222.
Wedemayer, G.J., Patten, P.A., Wang, L.H., Schultz, P.G., Stevens, R.C., 1997. Structural insights into the evolution of an antibody combining site. Science 276, 1665–1669.
Winn, M.D., Ballard, C.C., Cowtan, K.D., Dodson, E.J., Emsley, P., Evans, P.R., Keegan, R.M., Krissinel, E.B., Leslie, A.G., McCoy, A., McNicholas, S.J., Murshudov, G.N., Pannu, N.S., Potterton, E.A., Powell, H.R., Read, R.J., Vagin, A., Wilson, K.S., 2011. Overview of the CCP4 suite and current developments. Acta. Cryst D67, 235–242.
Yin, J., Mundorff, E.C., Yang, P.L., Wendt, K.U., Hanway, D., Stevens, R.C., Schultz, P.G., 2001. A comparative analysis of the immunological evolution of antibody 28B4. Biochemistry 40, 10764–10773.